

# Deoxyribonucleic Acid Encoded and Size-Defined $\pi$ -Stacking of Perylene Diimides

Jeffrey Gorman, Sarah R. E. Orsborne, Akshay Sridhar, Raj Pandya, Peter Budden, Alexander Ohmann, Naitik A. Panjwani, Yun Liu, Jake L. Greenfield, Simon Dowland, Victor Gray, Seán T. J. Ryan, Sara De Ornellas, Afaf H. El-Sagheer, Tom Brown, Jonathan R. Nitschke, Jan Behrends, Ulrich F. Keyser, Akshay Rao, Rosana Collepardo-Guevara, Eugen Stulz, Richard H. Friend,\* and Florian Auras\*



Cite This: *J. Am. Chem. Soc.* 2022, 144, 368–376



Read Online

ACCESS |



Metrics & More

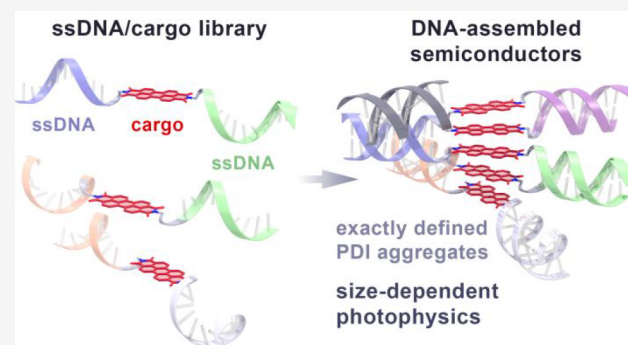


Article Recommendations



Supporting Information

**ABSTRACT:** Natural photosystems use protein scaffolds to control intermolecular interactions that enable exciton flow, charge generation, and long-range charge separation. In contrast, there is limited structural control in current organic electronic devices such as OLEDs and solar cells. We report here the DNA-encoded assembly of  $\pi$ -conjugated perylene diimides (PDIs) with deterministic control over the number of electronically coupled molecules. The PDIs are integrated within DNA chains using phosphoramidite coupling chemistry, allowing selection of the DNA sequence to either side, and specification of intermolecular DNA hybridization. In this way, we have developed a “toolbox” for construction of any stacking sequence of these semiconducting molecules. We have discovered that we need to use a full hierarchy of interactions: DNA guides the semiconductors into specified close proximity, hydrophobic–hydrophilic differentiation drives aggregation of the semiconductor moieties, and local geometry and electrostatic interactions define intermolecular positioning. As a result, the PDIs pack to give substantial intermolecular  $\pi$  wave function overlap, leading to an evolution of singlet excited states from localized excitons in the PDI monomer to excimers with wave functions delocalized over all five PDIs in the pentamer. This is accompanied by a change in the dominant triplet forming mechanism from localized spin–orbit charge transfer mediated intersystem crossing for the monomer toward a delocalized excimer process for the pentamer. Our modular DNA-based assembly reveals real opportunities for the rapid development of bespoke semiconductor architectures with molecule-by-molecule precision.



## INTRODUCTION

Plants and photosynthetic bacteria employ protein scaffolds to impose spatial control over a multitude of chlorophylls and carotenoids, dictating the energetic landscape and fate of photogenerated excitons and separated charge carriers.<sup>1–3</sup> However, such deterministic morphology control remains inaccessible for current organic electronic materials as used in organic light-emitting diodes, transistors, and photovoltaics.

Controlling the delocalization of excited states in artificial organic semiconductors is a key, unmet challenge. With classical self-assembly approaches, unrestricted self-aggregation of semiconductors precludes deterministic size-control of  $\pi$ -stacked molecules, leading to a distribution of molecular agglomerates instead.<sup>4,5</sup> While alternative covalent methods can confine two (or more) semiconductors into  $\pi$ -interacting arrangements,<sup>6–8</sup> their low synthetic yield and poor solubility of the products render these *de novo* methods inadequate for generating larger systems.

DNA nanotechnology provides a powerful means to repurpose double-helix formation for nanoconstruction.<sup>9,10</sup>

Base pairing between complementary single-stranded DNA (ssDNA) is stable, predictable, and high yielding, leading to programmable supramolecular architectures.<sup>11,12</sup> While nucleobases have optical band gaps too large for technological implementation as electronically active components, they are excellent scaffolds that can direct the assembly of attached cargos such as molecular semiconductors.<sup>13–18</sup>

DNA-mediated assembly of organic semiconductors, however, can be challenging because their hydrophobic aromatic backbone encourages self-aggregation.<sup>19</sup> This has limited semiconductor/DNA constructs mostly to weakly aggregating dyes such as cyanines at the cost of reduced electronic

Received: September 27, 2021

Published: December 22, 2021



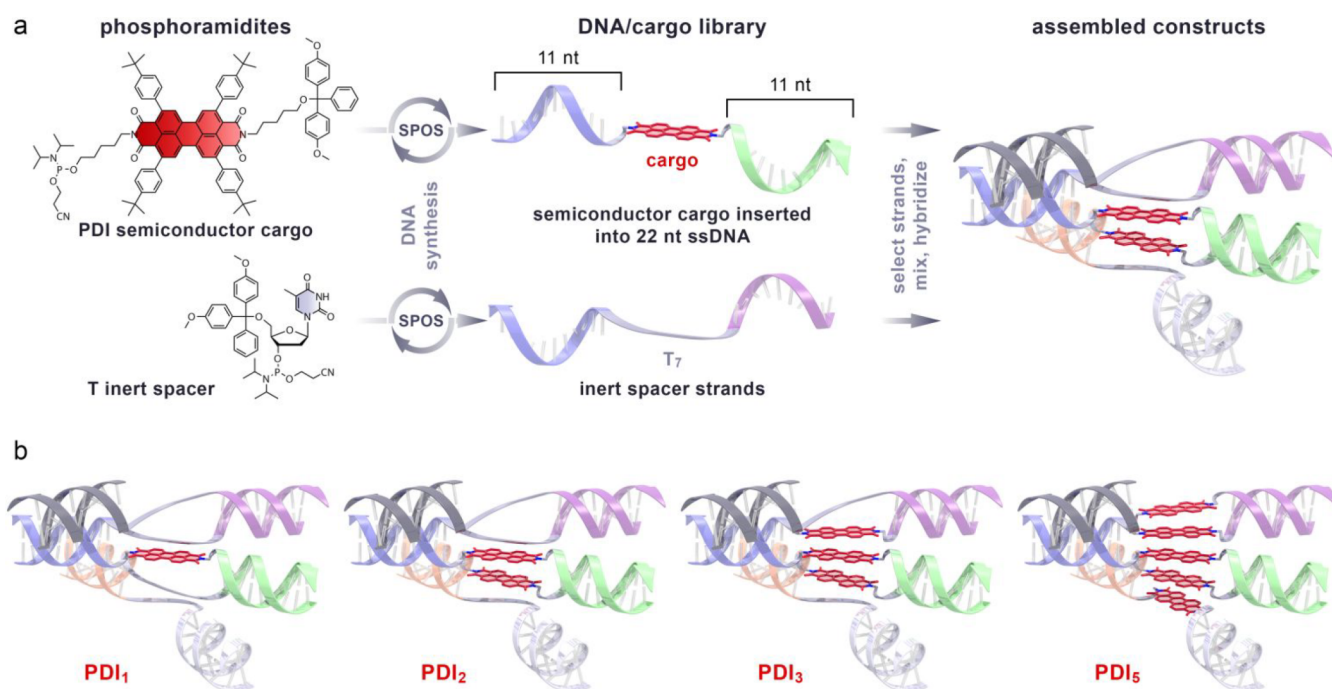


**Figure 1.** Assembling organic semiconductors via a DNA scaffold. (a) Asymmetric perylene diimide (PDI) phosphoramidites are conjugated to 22 nucleotide (nt) single-stranded DNA (ssDNA) by solid phase oligonucleotide synthesis (SPOS). Alternatively, heptathymine is employed as an electronically inert spacer. Repeating this process with different DNA sequences enables us to set up a cargo/DNA library with partially complementary ssDNA (color coding represents pairwise complementary base sequences). The final semiconductor/DNA constructs are assembled by selecting the desired components from this library, followed by hybridization to form rigid double-stranded DNA (dsDNA). (b) Schematic representation of the semiconductor/DNA constructs used in this study.

coupling.<sup>20,21</sup> However, these charged dyes are very different from the aromatic organic semiconductors employed in optoelectronic devices. To control the number of interacting dyes, previous approaches have mostly confined all dyes to a single DNA double helix.<sup>22,23</sup> However, if the dyes are incorporated instead of nucleobases, inserting several unnatural modifications can disrupt local base pairing and the double-helix structure.<sup>24,25</sup> Hence, examples of more than two  $\pi$ -stacked dyes assembled within one DNA double helix are rare. The other common strategy is the covalent attachment of dyes to the nucleobases. Here, the base pairing and duplex stability are less disrupted, enabling modifications of several adjacent base pairs, especially when a zipper-like arrangement is chosen.<sup>26</sup> However, since the dyes are positioned on the outside of the DNA double helix and are constrained to the DNA rotational pitch, their  $\pi$ -orbital overlap and electronic communication across multiple chromophores are limited.

We report here the DNA-encoded assembly of up to five  $\pi$ -conjugated perylene diimides (PDIs). These or an electronically inert spacer are integrated within DNA chains using phosphoramidite coupling chemistry, allowing selection of the DNA sequence to either side, and specification of intermolecular DNA hybridization. In this way, we have developed a “toolbox” for constructing bespoke semiconductor stacks with tailored electronic properties. Our approach facilitates extended PDI stacks with minimal base-pair disruption, compared to previous hairpin approaches.<sup>19,27</sup> We use a broad range of spectroscopic tools to track the temporal evolution of photogenerated excitons and their subsequent conversion into excimers and triplet states. Our modular DNA-based assembly reveals real opportunities for the rapid

development of customized semiconductor architectures with molecule-by-molecule precision.

## RESULTS AND DISCUSSION

The specificity of DNA base pairing enables the exact recognition between two complementary base sequences. ssDNA can share partial base-complementarity with several separate ssDNA strands, forming interconnected double stranded DNA (dsDNA) helices upon hybridization. This method of interconnecting dsDNA allows a combinatorial set of ssDNA to assemble into preprogrammed structures with nanometer resolution.

We adapted this method to generate precisely defined semiconductor/DNA constructs. Each construct consists of six zigzag interconnected dsDNA helices, formed by two 11-nucleotide (nt) “end-caps” and five partially complementary 22 nt cargo-modified ssDNA (Figure 1a and Supporting Information, Section C). The cargo is either a molecular semiconductor or heptathymine ( $T_7$ ) as an optically and electronically inert spacer. Importantly, the base sequences are specific to a position within the constructs, ensuring that the location of each cargo is programmable, and cargos are fully exchangeable. Perylene diimide (PDI) was chosen as a well-studied model semiconductor due to its chemical stability and strong tendency to  $\pi$ -stack. This approach overcomes previous limitations of dye–DNA base pair disruption by balancing duplex hybridization and hydrophobicity-driven dye assembly. Deploying a strategy where only one PDI molecule is attached per DNA strand, we leave base-pairing and duplex formation comparatively unimpeded. While the strong hydrophobicity of the PDIs is required as a driving force for structure assembly, aggregate size control is defined by two flanking DNA helices.

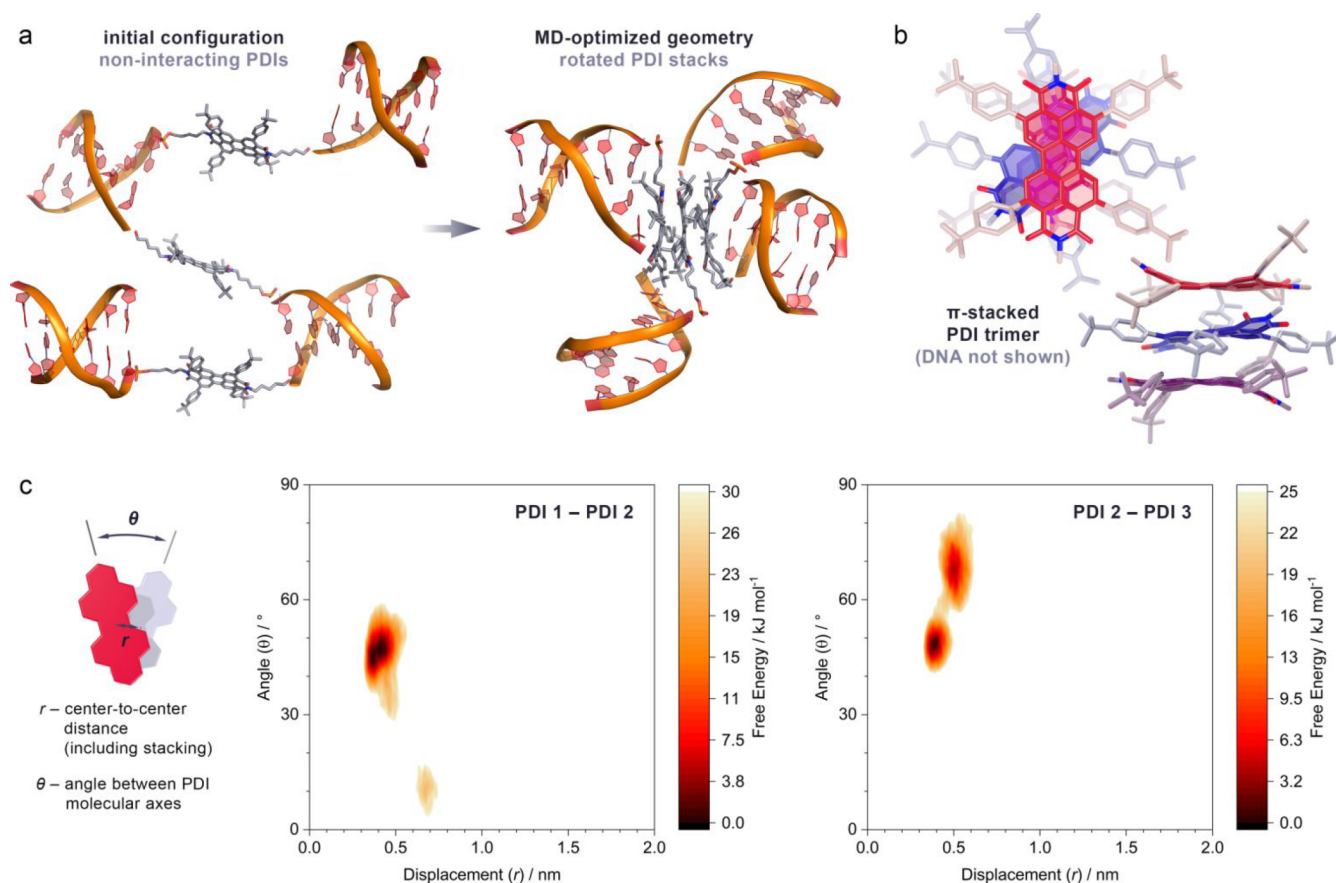


**Figure 2.** Structure simulations of a PDI trimer using atomistic molecular dynamics (MD) simulations with metadynamics sampling. (a) Comparison of the initial (left) and the minimum-energy configuration (right). (b) The optimized geometry features closely stacked PDIs where the middle one (blue) is rotated by about 45 deg. This configuration maximizes the overlap between the PDI cores while balancing the steric constraints due to the *tert*-butylphenyl substituents and the size mismatch between the dsDNA and the considerably smaller PDIs. Pentyl linkers and DNA are omitted for clarity. (c) MD-calculated free energy maps probing the angle  $\theta$  and the center-to-center distance  $r$  between the adjacent PDIs in the trimer. The energy scale is relative to the energy minimum. Despite different trajectories during the simulation where aggregation of one pair influences the other, both PDI pairs converge to the same global minimum around  $r = 0.4$  nm (i.e.,  $\pi$ -stacked with only small lateral offset) and  $\theta = 45^\circ$ .

Cargo-modified ssDNAs were prepared by sequential growth using phosphoramidite-based solid-phase oligonucleotide synthesis (SPOS) (SI, Section D). We chose phosphoramidite coupling over other bioconjugation strategies such as amide formation or copper(I)-catalyzed alkyne–azide cycloaddition (CuAAC), as the phosphoramidite route provides a short and geometrically simple connection between the cargo and DNA, and is compatible with strongly hydrophobic semiconductor cargos. Moreover, the sequential growth via SPOS ensures that the directionality of the DNA is maintained throughout each ssDNA-cargo-ssDNA strand. This is vital for the assembly of our semiconductor/DNA constructs, but very challenging to achieve via alternative amide or CuAAC approaches where the respective 3' and 5' modifiers are geometrically different.

After the synthesis of an initial 11 nucleotide (nt) ssDNA, the PDI cargo was inserted by a modified SPOS procedure, followed by another 11 nt ssDNA. Pentyl chains were employed as linkers to bridge the size disparity between the PDIs ( $\pi$ -stacking distance  $\approx 0.4$  nm) and the larger dsDNA helix diameter ( $\approx 2$  nm). In order to generate optically and electronically inert spacer strands, seven thymidine units were appended instead of the PDI cargo.

A cargo/DNA library was set up by generating the PDI- and T<sub>7</sub>-modified ssDNA strands for each position in the stack. To

generate the PDI/DNA constructs, the desired strands (one for each position) were selected from this library, followed by hybridization into dsDNA. Successful hybridization was confirmed by native polyacrylamide gel electrophoresis (PAGE) and temperature-dependent UV–vis spectroscopy (SI, Sections E, F). The constructs we chose for this study are shown in Figure 1b and range from the monomeric PDI<sub>1</sub> to an extended stack of PDIs in PDI<sub>5</sub>. The steric bulk and charge of the surrounding DNA ensure that in dilute solution all relevant electronic interactions are confined to the stacks with negligible crosstalk across neighboring constructs (SI, Section G).

While the DNA defines the number of PDIs per construct and dictates their general position within the stacks, the subnanometer scale arrangement is dominated by local interactions. In the highly polar aqueous environment, the PDIs aggregate due to hydrophobic/hydrophilic differentiation. The local geometry inside these aggregates is governed by electrostatic and dipole interactions and the 3D shape of the functionalized PDIs.

We developed structural models of the aggregated PDIs to both inform our construct design and support later photo-physical analysis. To characterize the conformational ensembles of cargo/DNA constructs, we performed atomistic



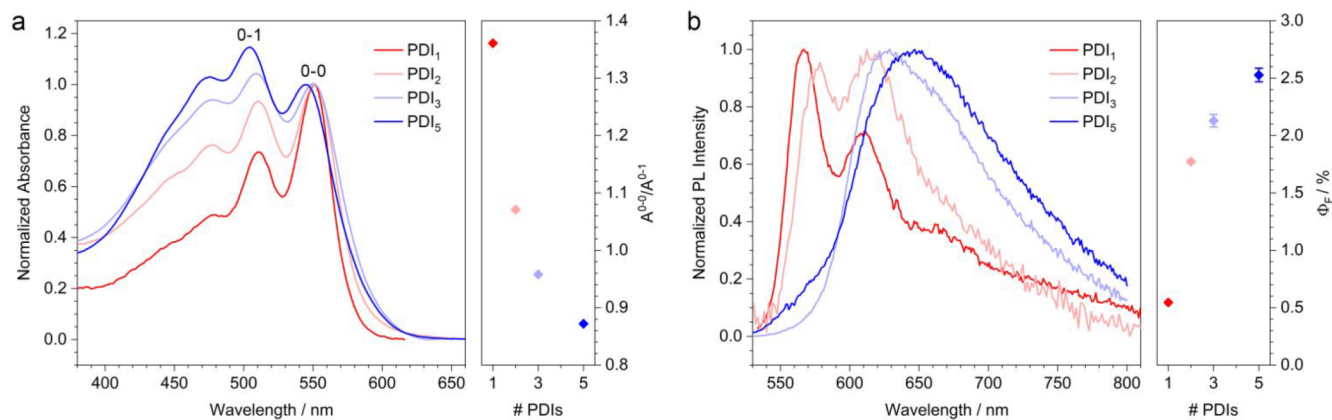


**Figure 3.** Steady-state optical characterization of the PDI/DNA constructs. (a) Absorption spectra of PDI<sub>1</sub>–PDI<sub>5</sub> (10–30  $\mu$ M in PBS), normalized to the absorbance of the 0–0 vibrational band. Right panel: Progressive H-aggregation with increasing number of PDIs per construct is evident from the absorption ratio between the 0–0 and 0–1 vibrational bands. (b) Photoluminescence (PL) emission spectra of the PDI/DNA constructs normalized to their respective maxima. The emission profiles change gradually from monomeric to excimer-like with increasing number of coupled PDIs. Right panel: The PL quantum efficiency ( $\phi_F$ ) increases with the number of PDIs due to suppressed competing relaxation pathways.

molecular dynamics (MD) simulations in combination with a well-tempered metadynamics algorithm for enhanced sampling.<sup>28,29</sup> We selected a PDI trimer with four 6 nt dsDNA as our main model system, since it allows us to probe cross-correlation of aggregated PDIs beyond a dimer but is sufficiently small to be simulated at the required level of theory (Figure 2a). See the SI, Section H for details and further simulations.

MD simulations were initialized with noninteracting PDIs ( $\geq 1.5$  nm separation) and proceed in 2 fs steps for 100 ns, driven by a history-dependent biasing potential to escape local minima. Prior MD simulations of similar-sized PDI-DNA base surrogates have demonstrated that the configurations typically converge in <10 ns and well before the 100 ns sampled here.<sup>30,31</sup> During the simulations, the PDIs and DNA are free to sample a wide range of configurations, including dsDNA dehybridization and variation of the PDI–PDI separation.

The PDI trimer converges to a cofacially stacked configuration which maximizes the electronic overlap between the PDIs (Figure 2a, b). The DNA helices remain fully hybridized.

In order to assess the stability of this arrangement, we computed the free energy maps for the center-to-center distance ( $r$ ) and the rotational offset ( $\theta$ ) between adjacent PDIs in the trimer (Figure 2c). In this simulation, the energy landscape is multidimensional as the aggregation of two PDIs influences the stacking interactions with the third PDI. Moreover, due to the directionality of the DNA, the trimer is not symmetric with PDI 1 being attached at the 5' end of the connecting dsDNA and PDI 3 at the 3' end. Hence, the energy maps are different for PDI 1–PDI 2 and PDI 2–PDI 3, respectively. The geometries corresponding to each of the observed minima are shown in the SI, Figure S7-2.

PDI 1–PDI 2 shows a clear preference for a 45° rotated arrangement with a center-to-center distance of about 0.4 nm, which approximates the typical distance between  $\pi$ -stacked PDIs with only minimal lateral offset. This rotated stacking motif is known from the solid-state structures of PDIs with bulky imide substituents.<sup>32</sup> A shallow local minimum is observed at  $r = 0.7$  nm/ $\theta = 10^\circ$ . This configuration resembles the slip-stacked solid-state structure of *ortho*-functionalized PDIs such as our monomer,<sup>33</sup> but appears significantly

destabilized in the PDI/DNA constructs due to the boundary conditions imposed by the sterically demanding DNA.

The PDI 2–PDI 3 pair assumes the same 45°-rotated,  $\pi$ -stacked arrangement as its most favorable geometry. A secondary minimum corresponds to a laterally displaced rotated stack with slightly reduced overlap between the PDI cores. This arrangement converts into the closely stacked configuration as the simulation proceeds.

Despite the inherent asymmetry of the PDI trimer due to the DNA directionality, both PDI pairs converge to the same geometry. This confirms that the above-described hierarchy of interactions leads to a specific and stable local geometry.

MD simulations carried out for a T<sub>7</sub>-flanked PDI dimer confirm that the PDI aggregation is not significantly altered by the addition of inert spacer strands (SI, Figure S7-1). Moreover, we simulated the geometry of the larger PDI<sub>5</sub> pentamer via computationally less expensive force-field methods (SI, Figure S7-3). The simulation reveals that PDI stacking is not hindered by the steric bulk of the six dsDNA. Indeed, the optimized configuration is very similar to the model PDI trimer with the PDIs adopting a 45° rotated, closely  $\pi$ -stacked arrangement.

The stacking geometry can have significant influence on the electronic communication across the PDI stacks. We quantified the electronic coupling by computing the singlet excitation energy transfer (SEET) integrals ( $t_s$ ) between adjacent PDIs via time-dependent density functional theory (TD-DFT), using the MD-optimized rotated stack or slip-stacked geometries. We find that  $t_s = 112$  meV for the rotated stack, which is comparable to the 80–150 meV reported for self-assembled PDIs,<sup>34,35</sup> confirming that the PDI/DNA constructs enable strong  $\pi$ – $\pi$  coupling. In contrast,  $t_s$  of the energetically less favorable (and experimentally not observed) slip-stacked geometry is only 53 meV, indicating significantly weaker electronic coupling.

The optical absorption spectra of PDIs are highly sensitive to aggregation effects, rendering these semiconductors an excellent probe for analyzing the DNA-encoded assembly. Modulation of the vibronic band intensities arises from a complex interplay between Coulomb and charge-transfer-mediated interactions that depend on the PDI–PDI spacing and local geometry.<sup>36,37</sup>

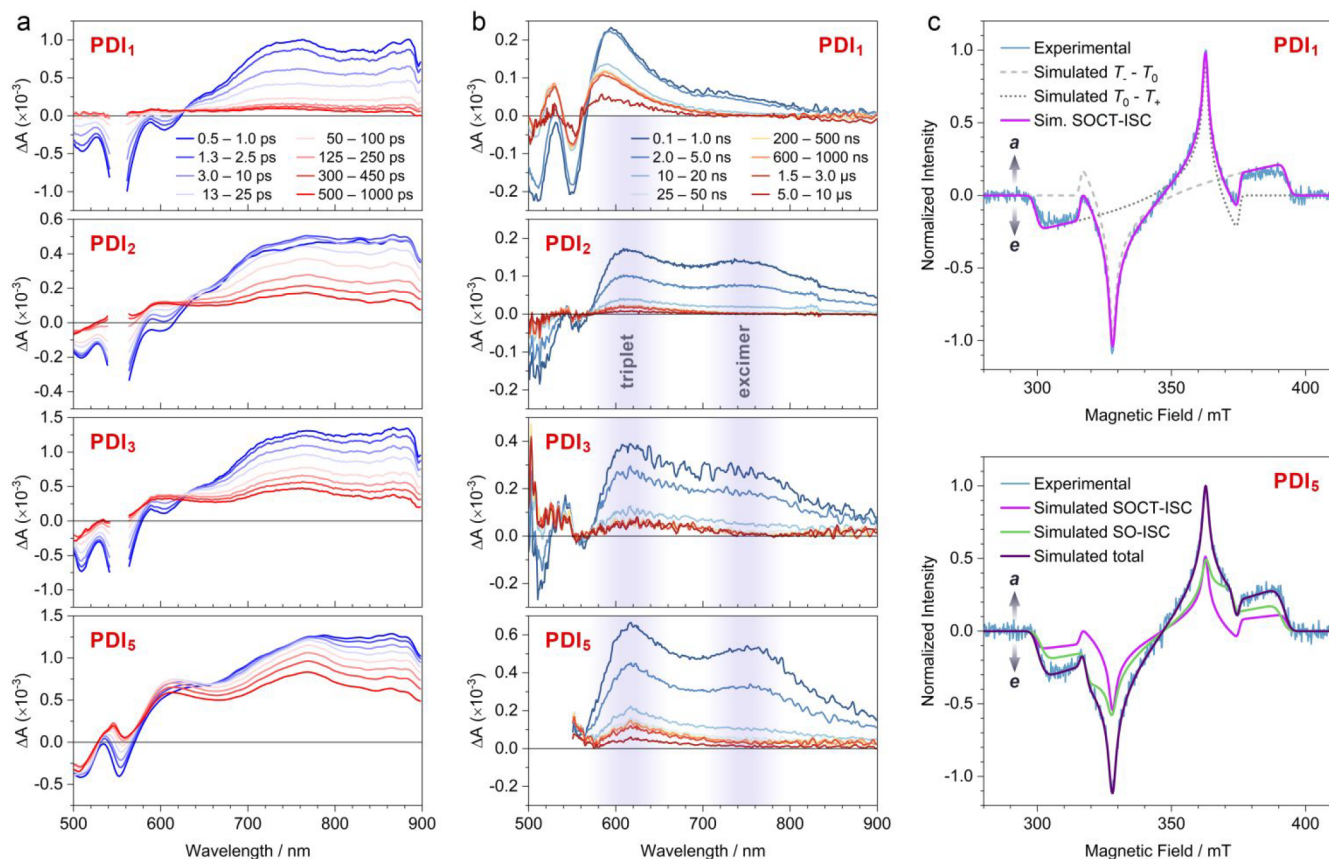


**Figure 4.** Time-resolved spectroscopy. (a) Femto-/picosecond transient absorption spectra of the PDI/DNA constructs (10–30  $\mu\text{M}$  in PBS). Excitation 550 nm, 24  $\mu\text{J cm}^{-2}$ . 540–560 nm removed due to pump scatter. (b) The corresponding nanosecond transient absorption spectra. Excitation 555 nm, 100  $\mu\text{J cm}^{-2}$ . (c) Transient EPR spectra of **PDI<sub>1</sub>** and **PDI<sub>5</sub>**, recorded at 100 K, time averaged 0.5–4  $\mu\text{s}$  after optical excitation at 532 nm. The trEPR spectrum of **PDI<sub>1</sub>** is well described by a triplet that is formed via a SOCT-ISC mechanism, giving rise to an *aeae/aea* ESP pattern (purple line). The dotted and dashed lines represent the simulated spectra of the  $T_- - T_0$  and  $T_0 - T_+$  components. The trEPR spectrum of **PDI<sub>5</sub>** requires two triplet species with different ESP patterns. The first one (purple line; 31% contribution) is a SOCT-ISC triplet with the same parameters as in **PDI<sub>1</sub>**, whereas the second one (green; 69% contribution) is formed via an excimer-based SO-ISC mechanism, which gives rise to an *eee/aaa* ESP pattern.

**PDI<sub>1</sub>** displays the typical vibronic progression of monomeric PDIs with a peak ratio between the 0–0 and 0–1 vibronic bands ( $A^{0-0}/A^{0-1}$ ) of >1.3 (Figure 3a).<sup>38</sup> The decreased vibronic peak ratio of **PDI<sub>2</sub>** indicates (relatively weak) H-coupling between the two PDIs. **PDI<sub>3</sub>** and **PDI<sub>5</sub>** show stronger H-aggregation with decreasing  $A^{0-0}/A^{0-1}$  peak ratio and blue-shifted absorption peaks. These observations support the anticipated (rotated) side-by-side stacking (as opposed to staircase arrangement) in our PDI/DNA constructs.<sup>39</sup> Moreover, the progressive aggregation effects in **PDI<sub>3</sub>** and **PDI<sub>5</sub>** confirm electronic coupling across the entire stacks.

The photoluminescence (PL) emission spectrum of **PDI<sub>1</sub>** mirrors its absorption spectrum, confirming the monomer-like properties of this construct (Figure 3b). The PL quantum efficiency ( $\phi_F$ ) is about 0.6%. Low  $\phi_F$  values are frequently observed for *ortho*-substituted PDIs and have been attributed to charge transfer (CT) from the phenylenes and increased out-of-plane vibrations promoting nonradiative decay pathways such as CT-mediated intersystem crossing (ISC) to triplets.<sup>40,41</sup> Consistent with this explanation, the  $\phi_F$  of the non-nucleic PDI diol 3 increases from 2.6% in solution to 23% in the solid state (SI, Section K).

With increasing number of coupled PDIs, the emission spectra become broader, featureless, and Stokes-shifted. This is

characteristic of PDI excimer emission ( $1^{*ex}\text{PDI}$ ), where the initial photoexcitation delocalizes over multiple chromophores, rearranging them into a lower-energy geometry, before decaying back to the ground state structure.<sup>42,43</sup> PDI excimers conventionally act as fluorescence traps. However, in our constructs, the rapid nonradiative losses that limit  $\phi_F$  in **PDI<sub>1</sub>** are outcompeted by the excimer formation, causing an overall increase in  $\phi_F$  from 0.6% (**PDI<sub>1</sub>**) to 2.5% (**PDI<sub>5</sub>**).

In order to track the evolution of excited states and investigate the impact of the PDI aggregate size, we employed a range of time-resolved spectroscopic techniques, specifically femto-/picosecond and nanosecond transient absorption spectroscopy (fs-TAS and ns-TAS, respectively), and transient electron paramagnetic resonance (trEPR) spectroscopy.

In TAS, photoexcitation of **PDI<sub>1</sub>–PDI<sub>5</sub>** generates ground state bleach (GSB) signals at 510 and 550 nm, and a short-lived stimulated emission (SE) signal at 605 nm (Figure 4a). Photoinduced absorption bands (PIA) are most prominent in the 630–900 nm range but can partially overlap with the GSB and SE at shorter wavelengths. While the GSB and SE signals are similar across the range of PDI/DNA constructs, the PIA bands and lifetimes of their components reveal significant differences.

Photoexcitation of  $\text{PDI}_1$  populates the singlet excited state ( $^1\text{PDI}$ ) with two overlapping PIA signals at 730 and 760 nm and an absorption band at 850–880 nm. The  $^1\text{PDI}$  signal decays within 500 ps and the GSB decays with approximately the same rate. Since the SE signal is small and significantly shorter-lived (<25 ps), we identify nonradiative internal conversion (IC) as the dominant decay pathway to the ground state. This is in line with the known tendency of *ortho*-phenyl substituents on PDIs to enhance out-of-plane vibrations, boosting nonradiative relaxation pathways and limiting  $\varphi_F$  as discussed above.

Concomitant with the  $^1\text{PDI}$  decay, we observe the appearance of a weak PIA band centered at 600 nm (partially overlapping with the remaining GSB), which decays slowly over  $>5 \mu\text{s}$  (Figure 4b). We assign this new species to a small population of nonemissive triplet states ( $^3\text{PDI}$ ), which are formed via intersystem crossing (ISC). This assignment is confirmed by triplet sensitization experiments (SI, Figure S9) and EPR (see below). Monomeric *ortho*-phenyl PDIs have previously been reported to increase the ISC rate through intramolecular charge-transfer interactions.<sup>44</sup> The triplet formation is also observed in the fs-TAS data of the PDI diol **3** in chloroform solution (SI, Section K).

In contrast to literature reports,<sup>27,45</sup> we do not observe the (in our case undesired) formation of a radical anion in  $\text{PDI}_1$  via photoinduced hole transfer to the purine nucleobases (A and G). We attribute this to the different geometry and linkage of our constructs, steric and electronic effects of the PDI *ortho*-substitution, and the short  $^1\text{PDI}$  lifetime (SI, Section L).

In the constructs that contain at least two electronically coupled PDIs the lifetime of excited states is significantly extended (Figure 4a). After 500 ps, about 25% of the  $\text{PDI}_2$  and  $\text{PDI}_3$  PIA, and more than 50% of the  $\text{PDI}_5$  PIA band intensity are still present. Moreover, changes in the PIA spectra reveal the population of different excited states when at least two PDIs are electronically coupled.

In  $\text{PDI}_5$ , where these differences are most prominent, a new state with a characteristic absorption band around 770 nm evolves within 1 ps (Figure 4a, bottom panel). The new state overlaps significantly with the GSB and SE bands at shorter wavelengths. In line with the findings from the steady-state PL spectroscopy, we assign this PIA to a singlet excimer state ( $^1\text{exPDI}$ )—the delocalization of the excited state over several coupled PDIs, which is accompanied by a structural relaxation to a new lower-energy excited state geometry. This assignment is further confirmed by EPR (see below). Tracking the evolution of the  $^1\text{PDI}$  850–880 nm band, we observe an interconversion of the short-lived  $^1\text{PDI}$  Frenkel excitons into the  $^1\text{exPDI}$ . The 770 nm excimer absorption persists for tens of nanoseconds (Figure 4b, bottom panel). Excimer formation is also observed in  $\text{PDI}_2$  and  $\text{PDI}_3$  with comparable lifetimes but lower  $\Delta A$ . The fs-TA spectra suggest the coexistence of  $^1\text{PDI}$  and  $^1\text{exPDI}$  at early times and incomplete conversion to the excimer (Figure 4a, middle panels). These findings are consistent with the trend observed in the steady-state PL spectra and the lower excimer yield according to the ns-TAS.

$\text{PDI}_2$ – $\text{PDI}_5$  display greatly enhanced triplet yields compared to  $\text{PDI}_1$ , as evident from the pronounced 600 nm PIA (Figure 4a,b). Higher triplet yields can be explained by the longer availability of singlet ( $^1\text{PDI}$  and  $^1\text{exPDI}$ ) states due to slower vibrational relaxation to ground state and hence more time for ISC, and a more efficient ISC mechanism via the excimer (see below).

We sought further confirmation of our above assignments from trEPR spectroscopy (Figure 4c). The trEPR spectrum of  $\text{PDI}_1$  shows a broad triplet feature with zero-field splitting (ZFS) parameters of  $D = 1314 \text{ MHz}$  and  $E = -115 \text{ MHz}$ , which are consistent with literature values for similar PDI systems.<sup>27</sup> The electron spin polarization (ESP) pattern is *eaе/aea*, where *e* = enhanced emission and *a* = enhanced absorption. Simulations of the triplet spectrum using the EasySpin software package<sup>46</sup> yield relative triplet sublevel populations of  $p_x, p_y, p_z = 0.18, 0.82, 0$ , indicating an overpopulation of the  $T_y$  zero-field eigenstate.

While the direct spin–orbit coupling mediated intersystem crossing (SO-ISC) from  $^1\text{PDI}$  to  $^3\text{PDI}$  is negligible in unsubstituted monomeric PDIs,<sup>47</sup> the intramolecular charge transfer (CT) interactions in *ortho*-substituted PDIs causes increased ISC rates and thus reduced  $\varphi_F$  as discussed above.<sup>40,41,44</sup> Consistent with this intramolecular CT character, the *eaе/aea* ESP pattern of  $\text{PDI}_1$  and overpopulation of the  $T_y$  sublevel suggest that the triplet formation proceeds through a spin–orbit charge transfer intersystem crossing (SOCT-ISC) mechanism.<sup>48–50</sup> SOCT-ISC leads to an overpopulation of  $T_y$  when  $D > 0$ , which is common in planar aromatic molecules, and  $E < 0$ . Furthermore, the absence of a clear CT state signal in the  $\text{PDI}_1$  trEPR spectrum indicates strong coupling between the donor and acceptor moieties in the singlet CT ( $^1\text{CT}$ ) state, which is known to facilitate SOCT-ISC.<sup>51</sup> Alternative triplet formation mechanisms such as radical pair ISC<sup>52</sup> or singlet fission<sup>53</sup> can be ruled out, since both mechanisms directly populate the high-field eigenstates, leading to, e.g., overpopulation of the  $T_0$  sublevel and giving rise to an *aeе/aeе* ESP pattern, for  $D > 0$ .

For the analysis of the  $\text{PDI}_5$  trEPR spectrum, we assume the same sign for the ZFS parameters as in  $\text{PDI}_1$ . However, a single triplet species does not fit the experimental data well. Besides the SOCT-ISC species (with the same ZFS parameters as for  $\text{PDI}_1$ ) we observe a second species with  $D = 1260 \text{ MHz}$ ,  $E = -93 \text{ MHz}$ , and  $p_x, p_y, p_z = 0.46, 0.54, 0$ . In this species, the more equal relative populations of the  $T_x$  and  $T_y$  sublevels and zero population of  $T_z$  leads to an *eeе/aaa* ESP pattern. Cofacial PDI aggregates have been reported to show triplet state generation through an excimer state with significant CT character ( $\text{PDI } \delta^-/\text{PDI } \delta^+$ ).<sup>43</sup> In these systems, the dominant triplet forming mechanism is an excimer-based spin–orbit coupling induced intersystem crossing (SO-ISC), which leads to the *eeе/aaa* ESP pattern observed in  $\text{PDI}_5$ .<sup>27</sup> The ZFS parameters of the SO-ISC species are also slightly smaller than those of the SOCT-ISC triplet, suggesting a more delocalized triplet state.

In  $\text{PDI}_5$ , the relative contributions of the excimer-based SO-ISC triplet and intramolecular SOCT-ISC triplet to the observed spectrum are 69% and 31%, respectively. A modified  $\text{PDI}_2$  displays the same two triplet species, but with 39% and 61% for the excimer-based SO-ISC and SOCT-ISC triplets, respectively (SI, Section M). This trend of excimer formation outcompeting intramolecular electronic processes as the number of electronically coupled PDIs increases is fully consistent with the progression observed in the PL and TAS spectra.

Upon further cooling, we observe a CT state (a narrow *a/e* signal around  $g = 2$ ) in the  $\text{PDI}_2$  and  $\text{PDI}_5$  samples, which we attribute to the partial CT character of the excimers (see the SI, Section M).



Overall, the exciton delocalization and excimer formation processes of PDI<sub>2</sub> align with previous PDI dimers restricted in DNA hairpins,<sup>27</sup> while our larger-order structures approximate the photophysical characteristics of their solid-state analogues.

## CONCLUSION

This work presents a method for rapid development of bespoke semiconductor architectures with molecular precision via DNA-encoded assembly. Using perylene diimide (PDI) as a representative example of strongly packing molecular semiconductors, we have discovered that we can achieve well-controlled aggregation by employing a hierarchy of interactions. While the DNA defines the overall layout on the nanometer scale, the exact intermolecular positioning is achieved via electrostatic and dipole interactions and the 3D geometry of the substituted PDIs. Our semiconductor/DNA constructs provide facile access to semiconductor stacks beyond the size limitations of conventional covalent chemistry approaches and enable systematic exploration of the size dependence of electronic processes. We illustrate the strength of this approach by studying the extension of singlet excited states from monomeric PDI to stacked PDI pentamers. With an increasing number of coupled PDIs, we observe a continuing spatial extension from localized excitons to excimers in which wave functions are delocalized over at least five PDI units. Our balanced hydrophobic-directed approach to assembly will be broadly extendable to most state-of-the-art optoelectronic materials, which share a lack of water-solubilizing moieties similar to PDI. The DNA-based assembly method will open up greater chemical design space to interrogate the size dependence of technologically important phenomena including singlet fission, triplet–triplet annihilation, and symmetry-breaking charge transfer in the future.

## ASSOCIATED CONTENT

### Supporting Information

The Supporting Information is available free of charge at <https://pubs.acs.org/doi/10.1021/jacs.1c10241>.

Experimental methods, synthetic procedures, structure analysis and additional spectroscopic data (PDF)

## AUTHOR INFORMATION

### Corresponding Authors

**Richard H. Friend** – Cavendish Laboratory, University of Cambridge, Cambridge CB3 0HE, United Kingdom; [orcid.org/0000-0001-6565-6308](https://orcid.org/0000-0001-6565-6308); Email: [rhf10@cam.ac.uk](mailto:rhf10@cam.ac.uk)

**Florian Auras** – Cavendish Laboratory, University of Cambridge, Cambridge CB3 0HE, United Kingdom; [orcid.org/0000-0003-1709-4384](https://orcid.org/0000-0003-1709-4384); Email: [fa355@cam.ac.uk](mailto:fa355@cam.ac.uk)

### Authors

**Jeffrey Gorman** – Cavendish Laboratory, University of Cambridge, Cambridge CB3 0HE, United Kingdom; [orcid.org/0000-0002-6888-7838](https://orcid.org/0000-0002-6888-7838)

**Sarah R. E. Orsborne** – Cavendish Laboratory, University of Cambridge, Cambridge CB3 0HE, United Kingdom

**Akshay Sridhar** – Department of Applied Physics, Science for Life Laboratory, KTH Royal Institute of Technology, 171 21 Solna, Sweden

**Raj Pandya** – Cavendish Laboratory, University of Cambridge, Cambridge CB3 0HE, United Kingdom; [orcid.org/0000-0003-1108-9322](https://orcid.org/0000-0003-1108-9322)

**Peter Budden** – Cavendish Laboratory, University of Cambridge, Cambridge CB3 0HE, United Kingdom

**Alexander Ohmann** – Cavendish Laboratory, University of Cambridge, Cambridge CB3 0HE, United Kingdom; [orcid.org/0000-0003-3537-1074](https://orcid.org/0000-0003-3537-1074)

**Naitik A. Panjwani** – Berlin Joint EPR Lab, Fachbereich Physik, Freie Universität Berlin, 14195 Berlin, Germany; [orcid.org/0000-0002-2913-5377](https://orcid.org/0000-0002-2913-5377)

**Yun Liu** – Cavendish Laboratory, University of Cambridge, Cambridge CB3 0HE, United Kingdom; [orcid.org/0000-0003-1630-4052](https://orcid.org/0000-0003-1630-4052)

**Jake L. Greenfield** – Yusuf Hamied Department of Chemistry, University of Cambridge, Cambridge CB2 1EW, United Kingdom

**Simon Dowland** – Cavendish Laboratory, University of Cambridge, Cambridge CB3 0HE, United Kingdom

**Victor Gray** – Department of Chemistry, Ångström Laboratory, Uppsala University, 751 20 Uppsala, Sweden; [orcid.org/0000-0001-6583-8654](https://orcid.org/0000-0001-6583-8654)

**Seán T. J. Ryan** – Cavendish Laboratory, University of Cambridge, Cambridge CB3 0HE, United Kingdom

**Sara De Ornellas** – Department of Chemistry, University of Oxford, Oxford OX1 3TA, United Kingdom

**Afaf H. El-Sagheer** – Department of Chemistry, University of Oxford, Oxford OX1 3TA, United Kingdom; [orcid.org/0000-0001-8706-1292](https://orcid.org/0000-0001-8706-1292)

**Tom Brown** – Department of Chemistry, University of Oxford, Oxford OX1 3TA, United Kingdom; [orcid.org/0000-0002-6538-3036](https://orcid.org/0000-0002-6538-3036)

**Jonathan R. Nitschke** – Yusuf Hamied Department of Chemistry, University of Cambridge, Cambridge CB2 1EW, United Kingdom; [orcid.org/0000-0002-4060-5122](https://orcid.org/0000-0002-4060-5122)

**Jan Behrends** – Berlin Joint EPR Lab, Fachbereich Physik, Freie Universität Berlin, 14195 Berlin, Germany; [orcid.org/0000-0003-1024-428X](https://orcid.org/0000-0003-1024-428X)

**Ulrich F. Keyser** – Cavendish Laboratory, University of Cambridge, Cambridge CB3 0HE, United Kingdom; [orcid.org/0000-0003-3188-5414](https://orcid.org/0000-0003-3188-5414)

**Akshay Rao** – Cavendish Laboratory, University of Cambridge, Cambridge CB3 0HE, United Kingdom; [orcid.org/0000-0003-4261-0766](https://orcid.org/0000-0003-4261-0766)

**Rosana Colleparado-Guevara** – Cavendish Laboratory, University of Cambridge, Cambridge CB3 0HE, United Kingdom; [orcid.org/0000-0003-1781-7351](https://orcid.org/0000-0003-1781-7351)

**Eugen Stulz** – Department of Chemistry & Institute for Life Sciences, University of Southampton, Highfield, Southampton SO17 1BJ, United Kingdom; [orcid.org/0000-0002-5302-2276](https://orcid.org/0000-0002-5302-2276)

Complete contact information is available at: <https://pubs.acs.org/doi/10.1021/jacs.1c10241>

## Notes

The authors declare no competing financial interest.

## ACKNOWLEDGMENTS

This project has received funding from the European Research Council (ERC) under the European Union's Horizon 2020 research and innovation programme (Grant Agreement No. 670405 and No. 803326) This work has been performed using

resources provided by the Cambridge Tier-2 system operated by the University of Cambridge Research Computing Service (<http://www.hpc.cam.ac.uk>), funded by the EPSRC Tier-2 capital grant EP/P020259/1. A.S. and R.C.G. thank funding from the Winton Advanced Research Programme for the Physics of Sustainability. R.H.F. and Y.L. acknowledge support from the Simons Foundation (Grant 601946). V.G. acknowledges funding from the Swedish research council, Vetenskapsrådet 2018-00238. The authors thank Andrew J. Musser for fruitful discussions.

## REFERENCES

- (1) Engel, G. S.; Calhoun, T. R.; Read, E. L.; Ahn, T.-K.; Mancal, T.; Cheng, Y.-C.; Blankenship, R. E.; Fleming, G. R. Evidence for wavelike energy transfer through quantum coherence in photo-synthetic systems. *Nature* **2007**, *446*, 782–786.
- (2) Scholes, G. D.; Fleming, G. R.; Olaya-Castro, A.; van Grondelle, R. Lessons from nature about solar light harvesting. *Nat. Chem.* **2011**, *3*, 763–774.
- (3) Brédas, J.-L.; Sargent, E. H.; Scholes, G. D. Photovoltaic concepts inspired by coherence effects in photosynthetic systems. *Nat. Mater.* **2017**, *16*, 35–44.
- (4) Kaiser, T. E.; Wang, H.; Stepanenko, V.; Würthner, F. Supramolecular Construction of Fluorescent J-Aggregates Based on Hydrogen-Bonded Perylene Dyes. *Angew. Chem., Int. Ed.* **2007**, *46*, 5541–5544.
- (5) Chen, Z.; Lohr, A.; Saha-Möller, C. R.; Würthner, F. Self-assembled p-stacks of functional dyes in solution: structural and thermodynamic features. *Chem. Soc. Rev.* **2009**, *38*, 564–584.
- (6) Hayes, D.; Griffin, G. B.; Engel, G. S. Engineering Coherence Among Excited States in Synthetic Heterodimer Systems. *Science* **2013**, *340*, 1431–1434.
- (7) Margulies, E. A.; Shoer, L. E.; Eaton, S. W.; Wasielewski, M. R. Excimer formation in cofacial and slip-stacked perylene-3,4:9,10-bis(dicarboximide) dimers on a redox-inactive triptycene scaffold. *Phys. Chem. Chem. Phys.* **2014**, *16*, 23735–23742.
- (8) Margulies, E. A.; Miller, C. E.; Wu, Y.; Ma, L.; Schatz, G. C.; Young, R. M.; Wasielewski, M. R. Enabling singlet fission by controlling intramolecular charge transfer in  $\pi$ -stacked covalent terylenediimide dimers. *Nat. Chem.* **2016**, *8*, 1120–1125.
- (9) Seeman, N. C. Nucleic Acid Junctions and Lattices. *J. Theor. Biol.* **1982**, *99*, 237–247.
- (10) Rothmund, P. W. K. Folding DNA to create nanoscale shapes and patterns. *Nature* **2006**, *440*, 297–302.
- (11) Ong, L. L.; Hanikel, N.; Yaghi, O. K.; Grun, C.; Strauss, M. T.; Bron, P.; Lai-Kee-Him, J.; Schueder, F.; Wang, B.; Wang, P.; Kishi, J. Y.; Myhrvold, C.; Zhu, A.; Jungmann, R.; Bellot, G.; Ke, Y.; Yin, P. Programmable self-assembly of three-dimensional nanostructures from 10,000 unique components. *Nature* **2017**, *552*, 72–77.
- (12) Tikhomirov, G.; Petersen, P.; Qian, L. Fractal assembly of micrometre-scale DNA origami arrays with arbitrary patterns. *Nature* **2017**, *552*, 67–71.
- (13) Mirkin, C. A.; Letsinger, R. L.; Mucic, R. C.; Storhoff, J. J. A DNA-based method for rationally assembling nanoparticles into macroscopic materials. *Nature* **1996**, *382*, 607–609.
- (14) Gartner, Z. J.; Liu, D. R. The Generality of DNA-Templated Synthesis as a Basis for Evolving Non-Natural Small Molecules. *J. Am. Chem. Soc.* **2001**, *123*, 6961–6963.
- (15) Malinovskii, V. L.; Wenger, D.; Häner, R. Nucleic acid-guided assembly of aromatic chromophores. *Chem. Soc. Rev.* **2010**, *39*, 410–422.
- (16) Kuzyk, A.; Schreiber, R.; Fan, Z.; Pardatscher, G.; Roller, E.-M.; Högele, A.; Simmel, F. C.; Govorov, A. O.; Liedl, T. DNA-based self-assembly of chiral plasmonic nanostructures with tailored optical response. *Nature* **2012**, *483*, 311–314.
- (17) Ensslen, P.; Wagenknecht, H.-A. One-Dimensional Multi-chromophore Arrays Based on DNA: From Self-Assembly to Light-Harvesting. *Acc. Chem. Res.* **2015**, *48*, 2724–2733.
- (18) Stulz, E. Nanoarchitectonics with Porphyrin Functionalized DNA. *Acc. Chem. Res.* **2017**, *50*, 823–831.
- (19) Winiger, C. B.; Langenegger, S. M.; Calzaferri, G.; Häner, R. Formation of Two Homo-chromophoric H-Aggregates in DNA-Assembled Alternating Dye Stacks. *Angew. Chem., Int. Ed.* **2015**, *54*, 3643–3647.
- (20) Boulais, É.; Sawaya, N. P. D.; Veneziano, R.; Andreoni, A.; Banal, J. L.; Kondo, T.; Mandal, S.; Lin, S.; Schlau-Cohen, G. S.; Woodbury, N. W.; Yan, H.; Aspuru-Guzik, A.; Bathe, M. Programmed coherent coupling in a synthetic DNA-based excitonic circuit. *Nat. Mater.* **2018**, *17*, 159–166.
- (21) Zhou, X.; Mandal, S.; Jiang, S.; Lin, S.; Yang, J.; Liu, Y.; Whitten, D. G.; Woodbury, N. W.; Yan, H. Efficient Long-Range, Directional Energy Transfer through DNATemplated Dye Aggregates. *J. Am. Chem. Soc.* **2019**, *141*, 8473–8481.
- (22) Fendt, L.-A.; Bouamaied, I.; Thöni, S.; Amiot, N.; Stulz, E. DNA as Supramolecular Scaffold for Porphyrin Arrays on the Nanometer Scale. *J. Am. Chem. Soc.* **2007**, *129*, 15319–15329.
- (23) Mayer-Enthart, E.; Wagner, C.; Barbaric, J.; Wagenknecht, H.-A. Helical self-assembled chromophore clusters based on DNA-like architecture. *Tetrahedron* **2007**, *63*, 3434–3439.
- (24) Takada, T.; Ashida, A.; Nakamura, M.; Fujitsuka, M.; Majima, T.; Yamana, K. Photocurrent Generation Enhanced by Charge Delocalization over Stacked Perylenediimide Chromophores Assembled within DNA. *J. Am. Chem. Soc.* **2014**, *136*, 6814–6817.
- (25) Kashida, H.; Sekiguchi, K.; Liang, X.; Asanuma, H. Accumulation of Fluorophores into DNA Duplexes To Mimic the Properties of Quantum Dots. *J. Am. Chem. Soc.* **2010**, *132*, 6223–6230.
- (26) Nguyen, T.; Brewer, A.; Stulz, E. Duplex Stabilization and Energy Transfer in Zipper Porphyrin–DNA. *Angew. Chem., Int. Ed.* **2009**, *48*, 1974–1977.
- (27) Carmieli, R.; Zeidan, T. A.; Kelley, R. F.; Mi, Q.; Lewis, F. D.; Wasielewski, M. R. Excited State, Charge Transfer, and Spin Dynamics in DNA Hairpin Conjugates with Perylenediimide Hairpin Linkers. *J. Phys. Chem. A* **2009**, *113*, 4691–4700.
- (28) Laio, A.; Parrinello, M. Escaping free-energy minima. *Proc. Natl. Acad. Sci. U. S. A.* **2002**, *99*, 12562–12566.
- (29) Barducci, A.; Bussi, G.; Parrinello, M. Well-Tempered Metadynamics: A Smoothly Converging and Tunable Free-Energy Method. *Phys. Rev. Lett.* **2008**, *100*, 020603.
- (30) Markegard, C. B.; Mazaheripour, A.; Jocson, J.-M.; Burke, A. M.; Dickson, M. N.; Gorodetsky, A. A.; Nguyen, H. D. Molecular Dynamics Simulations of Perylenediimide DNA Base Surrogates. *J. Phys. Chem. B* **2015**, *119*, 11459–11465.
- (31) Bartlett, A.; Markegard, C. B.; Dibble, D. J.; Gorodetsky, A. A.; Sharifzadeh, S.; Nguyen, H. D. Molecular dynamics simulations of DNA-inspired macromolecules from perylenediimide base surrogates. *Synth. Met.* **2019**, *253*, 146–152.
- (32) Austin, A.; Hestand, N. J.; McKendry, I. G.; Zhong, C.; Zhu, X.; Zdilla, M. J.; Spano, F. C.; Szarko, J. M. Enhanced Davydov Splitting in Crystals of a Perylene Diimide Derivative. *J. Phys. Chem. Lett.* **2017**, *8*, 1118–1123.
- (33) Eaton, S. W.; Shoer, L. E.; Karlen, S. D.; Dyar, S. M.; Margulies, E. A.; Veldkamp, B. S.; Ramanan, C.; Hartzler, D. A.; Savikhin, S.; Marks, T. J.; Wasielewski, M. R. Singlet Exciton Fission in Polycrystalline Thin Films of a Slip-Stacked Perylenediimide. *J. Am. Chem. Soc.* **2013**, *135*, 14701–14712.
- (34) Idé, J.; Méreau, R.; Ducasse, L.; Castet, F.; Olivier, Y.; Martinelli, N.; Cornil, J.; Beljonne, D. Supramolecular Organization and Charge Transport Properties of Self-Assembled  $\pi$ - $\pi$  Stacks of Perylene Diimide Dyes. *J. Phys. Chem. B* **2011**, *115*, 5593–5603.
- (35) Hestand, N. J.; Spano, F. C. Interference between Coulombic and CT-mediated couplings in molecular aggregates: H- to J-aggregate transformation in perylene-based  $\pi$ -stacks. *J. Chem. Phys.* **2015**, *143*, 244707.
- (36) Hestand, N. J.; Spano, F. C. Molecular Aggregate Photophysics beyond the Kasha Model: Novel Design Principles for Organic Materials. *Acc. Chem. Res.* **2017**, *50*, 341–350.



(37) Oleson, A.; Zhu, T.; Dunn, I. S.; Bialas, D.; Bai, Y.; Zhang, W.; Dai, M.; Reichman, D. R.; Tempelaar, R.; Huang, L.; Spano, F. C. Perylene Diimide-Based H<sub>j</sub>- and h<sub>j</sub>-Aggregates: The Prospect of Exciton Band Shape Engineering in Organic Materials. *J. Phys. Chem. C* **2019**, *123*, 20567–20578.

(38) Kaufmann, C.; Bialas, D.; Stolte, M.; Würthner, F. Discrete  $\pi$ -Stacks of Perylene Bisimide Dyes within Folda-Dimers: Insight into Long- and Short-Range Exciton Coupling. *J. Am. Chem. Soc.* **2018**, *140*, 9986–9995.

(39) Lim, J. M.; Kim, P.; Yoon, M.-C.; Sung, J.; Dehm, V.; Chen, Z.; Würthner, F.; Kim, D. Exciton delocalization and dynamics in helical p-stacks of self-assembled perylene bisimides. *Chem. Sci.* **2013**, *4*, 388–397.

(40) Nakazono, S.; Easwaramoorthi, S.; Kim, D.; Shinokubo, H.; Osuka, A. Synthesis of Arylated Perylene Bisimides through C-H Bond Cleavage under Ruthenium Catalysis. *Org. Lett.* **2009**, *11*, 5426–5429.

(41) Shoer, L. E.; Eaton, S. W.; Margulies, E. A.; Wasielewski, M. R. Photoinduced Electron Transfer in 2,5,8,11-Tetrakis-Donor-Substituted Perylene-3,4:9,10-bis(dicarboximides). *J. Phys. Chem. B* **2015**, *119*, 7635–7643.

(42) Schubert, A.; Settels, V.; Liu, W.; Würthner, F.; Meier, C.; Fink, R. F.; Schindlbeck, S.; Lochbrunner, S.; Engels, B.; Engel, V. Ultrafast Exciton Self-Trapping upon Geometry Deformation in Perylene-Based Molecular Aggregates. *J. Phys. Chem. Lett.* **2013**, *4*, 792–796.

(43) Veldman, D.; Chopin, S. M. A.; Meskers, S. C. J.; Groeneveld, M. M.; Williams, R. M.; Janssen, R. A. J. Triplet Formation Involving a Polar Transition State in a Well-Defined Intramolecular Perylenediimide Dimeric Aggregate. *J. Phys. Chem. A* **2008**, *112*, 5846–5857.

(44) Yu, Z.; Wu, Y.; Peng, Q.; Sun, C.; Chen, J.; Yao, J.; Fu, H. Accessing the Triplet State in Heavy-Atom-Free Perylene Diimides. *Chem. - Eur. J.* **2016**, *22*, 4717–4722.

(45) Takada, T.; Ido, M.; Ashida, A.; Nakamura, M.; Fujitsuka, M.; Kawai, K.; Majima, T.; Yamana, K. Photocurrent Generation through Charge-Transfer Processes in Noncovalent Perylenediimide/DNA Complexes. *Chem. - Eur. J.* **2015**, *21*, 6846–6851.

(46) Stoll, S.; Schweiger, A. EasySpin, a comprehensive software package for spectral simulation and analysis in EPR. *J. Magn. Reson.* **2006**, *178*, 42–55.

(47) Kircher, T.; Löhmansröben, H.-G. Photoinduced charge recombination reactions of a perylene dye in acetonitrile. *Phys. Chem. Chem. Phys.* **1999**, *1*, 3987–3992.

(48) Dance, Z. E. X.; Mickle, S. M.; Wilson, T. M.; Ricks, A. B.; Scott, A. M.; Ratner, M. A.; Wasielewski, M. R. Intersystem Crossing Mediated by Photoinduced Intramolecular Charge Transfer: Julolidine–Anthracene Molecules with Perpendicular  $\pi$  Systems. *J. Phys. Chem. A* **2008**, *112*, 4194–4201.

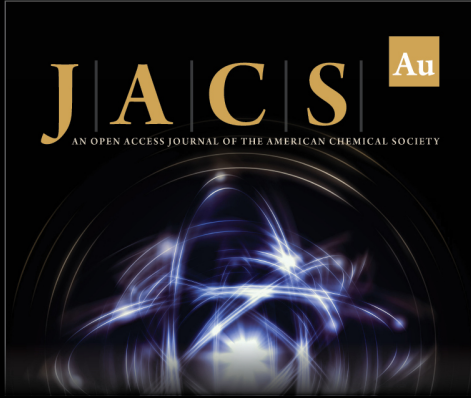
(49) van Willigen, H.; Jones, G.; Farahat, M. S. Time-Resolved EPR Study of Photoexcited Triplet-State Formation in Electron-Donor-Substituted Acridinium Ions. *J. Phys. Chem.* **1996**, *100*, 3312–3316.

(50) Okada, T.; Karaki, I.; Matsuzawa, E.; Mataga, N.; Sakata, Y.; Misumi, S. Ultrafast intersystem crossing in some intramolecular heteroexcimers. *J. Phys. Chem.* **1981**, *85*, 3957–3960.

(51) Miura, T.; Carmieli, R.; Wasielewski, M. R. Time-Resolved EPR Studies of Charge Recombination and Triplet-State Formation within Donor–Bridge–Acceptor Molecules Having Wire-Like Oligofluorene Bridges. *J. Phys. Chem. A* **2010**, *114*, 5769–5778.


(52) Levanon, H.; Norris, J. R. The photoexcited triplet state and photosynthesis. *Chem. Rev.* **1978**, *78*, 185–198.


(53) Weiss, L. R.; Bayliss, S. L.; Kraffert, F.; Thorley, K. J.; Anthony, J. E.; Bittl, R.; Friend, R. H.; Rao, A.; Greenham, N. C.; Behrends, J. Strongly exchange-coupled triplet pairs in an organic semiconductor. *Nat. Phys.* **2017**, *13*, 176–181.



**JACS** Au  
AN OPEN ACCESS JOURNAL OF THE AMERICAN CHEMICAL SOCIETY

Editor-in-Chief  
**Prof. Christopher W. Jones**  
Georgia Institute of Technology, USA

**Open for Submissions** 

pubs.acs.org/jacsau  ACS Publications  
Most Trusted. Most Cited. Most Read.